Applied Physics Letters

Probing the effect of interface on vortex pinning efficiency of one-dimensional $BaZrO_3$ and $BaHfO_3$ artificial pinning centers in $YBa_2Cu_3O_{7-x}$ thin films

Cite as: Appl. Phys. Lett. **113**, 212602 (2018); https://doi.org/10.1063/1.5050616
Submitted: 01 August 2018 . Accepted: 05 November 2018 . Published Online: 19 November 2018

Bibek Gautam, Mary Ann Sebastian, Shihong Chen, Shikhar Misra, Jijie Huang, F. Javier Baca, Rose Emergo, Timothy Haugan, Zhongwen Xing, Haiyan Wang, and Judy Z. Wu

Probing the effect of interface on vortex pinning efficiency of one-dimensional $BaZrO_3$ and $BaHfO_3$ artificial pinning centers in $YBa_2Cu_3O_{7-x}$ thin films

Bibek Gautam,[1,a)] Mary Ann Sebastian,[2] Shihong Chen,[1,3] Shikhar Misra,[4] Jijie Huang,[4] F. Javier Baca,[1] Rose Emergo,[1] Timothy Haugan,[2] Zhongwen Xing,[3] Haiyan Wang,[4] and Judy Z. Wu[1,a)]

[1]*Department of Physics and Astronomy, University of Kansas, Lawrence, Kansas 66045, USA*
[2]*U.S. Air Force Research Laboratory, Aerospace Systems Directorate, WPAFB, Ohio 45433, USA*
[3]*College of Engineering and Applied Science, Nanjing University, Nanjing, Jiangsu 210093, China*
[4]*School of Materials Engineering, Purdue University, West Lafayette, Indiana 47907, USA*

(Received 1 August 2018; accepted 5 November 2018; published online 19 November 2018)

C-axis-aligned one-dimensional artificial pinning centers (1D-APCs) provide strong correlated pinning of magnetic vortices and enhance critical current density J_c in superconducting $YBa_2Cu_3O_{7-x}$ (YBCO) films and coated conductors. A fundamental question arises on what determines the pinning efficiency of different 1D-APCs. To shed light on this question, this work investigates the correlation between the 1D-APC/YBCO interface and the pinning efficiency of 1D-APCs of $BaHfO_3$ (BHO) and $BaZrO_3$ (BZO) of comparable diameters of 5–6 nm. Intriguingly, a highly coherent BHO 1D-APC/YBCO interface is revealed even at a high BHO doping level of 6 vol. %, in contrast to a semi-coherent BZO 1D-APC/YBCO interface with a large number of dislocations. This leads to a profound effect on the pinning efficiency of these 1D-APCs. Specifically, a record high pinning force density peak $F_{p,max} \sim 182.0\ GN\,m^{-3}$ at $H_{max} > 9.0\,T$ and 65 K is obtained in the former, which is 2.5 times of the best reported in the latter. Moreover, a ratio of H_{max} to accommodation field H^* determined from the 1D-APC areal concentration is found up to 3.5 in the former in contrast to 0.7 in the latter, demonstrating the critical impact of the APC/YBCO interface on the pinning efficiency of 1D-APCs. *Published by AIP Publishing.* https://doi.org/10.1063/1.5050616

Nanoscale artificial pinning centers (APCs) can provide effective pinning of quantized magnetic vortices in high temperature superconductors (HTSs), particularly $REBaCu_3O_{7-x}$ (REBCO, RE = Y, Gd, and Sm) films and coated conductors, and therefore enhance the critical current density (J_c), which is crucial to practical applications of HTS electronic and electrical devices and systems.[1–3] Several materials have been reported to self-assemble into 1D-APCs along the *c*-axis of REBCO during growth and therefore provide a strong correlated pinning of the vortices when the applied magnetic field H is along the axial direction of the 1D-APCs. These *c*-axis aligned 1D-APCs are particularly important to REBCO, or HTSs in general, to address the pinning anisotropy associated with the layered structures of HTSs, resulting in the weakest pinning at the $H//c$-axis. The materials that form *c*-axis aligned 1D-APCs include $BaZrO_3$ (BZO),[3,4] $BaSnO_3$ (BSO),[3,5,6] $BaHfO_3$ (BHO),[7] and $YBa_2(Nb/Ta)O_6$.[8] The enhancement of J_c by these *c*-axis aligned 1D-APCs is often illustrated as a J_c peak at the $H//c$-axis in 1D-APC/REBCO nanocomposite samples.

Quantitatively, the pinning efficiency of the 1D-APCs has not been studied systematically and may be affected by their morphology, dimension, and interface with the REBCO matrix. Using an elastic energy model,[9,10] some insights have been obtained on how the elastic properties of the APC and REBCO matrix materials, APC and REBCO lattice mismatches, APC doping concentration, and processing conditions may affect the APC's morphology and dimension.[2,11] In particular, it was found that the elastic properties of the APC and REBCO matrix materials play a deterministic role in the diameter of the 1D-APCs.[12] This finding is consistent with experimental results, especially the comparable diameter on the order of 5–6 nm for the BHO and BZO 1D-APCs in REBCO matrices, despite a lower structural rigidity of the BHO APCs[13] which leads to a more adaptive behavior to the local strain generated by a secondary Y_2O_3 APC doping.[9] The higher adaptivity, together with a lower BHO 1D-APC/$YBa_2Cu_3O_{7-x}$ (YBCO) interface energy, is anticipated from the smaller lattice mismatch as compared to that of the BZO/YBCO (Table S1 in the supplementary material). This raises a fundamental question on how these properties would impact the BHO 1D-APC/YBCO and BZO 1D-APC/YBCO interfaces and to what extent the interfaces would affect the pinning efficiency of the individual BHO and BZO 1D-APCs of similar morphology and dimension.

To shed light on these important questions, this work presents a study of the 2–6 vol. % BHO 1D-APC/YBCO and BZO 1D-APC/YBCO nanocomposite films by combining the transport J_c measurement at 65–77 K and H up to 9.0 T and high-resolution transmission electron microscopy (HRTEM) of the 1D-APC morphology (Figs. S1 and S2 and Table S1 in the supplementary material) and interface with YBCO. This allows a quantitative probe on how the pinning efficiency is evaluated from the maximum value ($F_{p,max}$) of the force density $\boldsymbol{F_p} = \boldsymbol{J_c} \times \boldsymbol{H}$ and its location at H_{max}. The ratio between H_{max} and HRTEM determined accommodation field $H^* = n^*\Phi_o$, where n^* is the areal concentration of the 1D-APC and Φ_o is the flux quantum ($\sim 2.07 \times 10^{-15}$ Wb), provides a further quantitative probe on the pinning efficiency of BHO and BZO 1D-APCs. Intriguingly, a coherent

a)Electronic addresses: gautbibe@ku.edu and jwu@ku.edu

BHO 1D-APC/YBCO interface is revealed in the entire BHO doping range, in contrast to a semi-coherent BZO 1D-APC/YBCO interface due to the formation of the interfacial dislocations, resulting in a fundamental difference in the individual pinning efficiency of BHO and BZO 1D-APCs. In particular, the significantly higher $F_{p,max}$ by a factor of 250%–510% and a higher H_{max}/H^* ratio of by a factor of 350%–500% are observed on the BHO 1D-APCs as compared to those of the BZO 1D-APCs. It illustrates a critical impact of the 1D-APC/YBCO interface on the pinning efficiency of the 1D-APCs.

Figure 1 depicts the HRTEM and fast Fourier filtered images on 4 vol. % BZO 1D-APC/YBCO [Figs. 1(a) and 1(d)], 4 vol. % BHO 1D-APC/YBCO [Figs. 1(b) and 1(e)], and 6 vol. % BHO 1D-APC/YBCO [Figs. 1(c) and 1(f)] samples. The fast Fourier filtered images in Figs. 1(d)–1(f) are processed based on the following steps: first, the area of interests was first selected in the TEM image, and a fast Fourier transform (FFT) process of the area was conducted. By selecting and masking the specific diffraction dots in the FFT, the masked FFT was inverted to the fast Fourier filtered images as shown in Figs. 1(d)–1(f). A major difference between the two cases is in the higher concentration of dislocations (white marks) at the BZO 1D-APC/YBCO interface, which may be explained by the larger lattice mismatch (Table S1) and higher rigidity of BZO.[9,10] A direct consequence of the high interfacial defect concentration is the strain release in a short range of 1–2 nm from the interface, in which considerable oxygen deficiency was confirmed.[14] While a longer-range strain remains, it is less intensive and renders much smaller *ab*-plane buckling in the YBCO matrix away from the interface as supported by the comparable *c*-axis lattice constant to that of undoped YBCO (Fig. S1 and Table S1). In contrast, the BHO/YBCO interface is otherwise coherent, but a few randomly distributed dislocations and significant *ab*-plane buckling can be observed. This indicates that the BHO and YBCO lattices adapt to each other, which is supported by the nearly constant *c*-axis lattice constant ~11.77 Å-11.78 Å for all BHO 1D-APC/YBCO samples shown in Fig. S1 and Table S1, resulting in a long-range strain field in the BHO 1D-APC/YBCO nanocomposite film. Such high density plane-buckling was confirmed by the stripped diffraction dots in the BHO-samples. Interestingly,

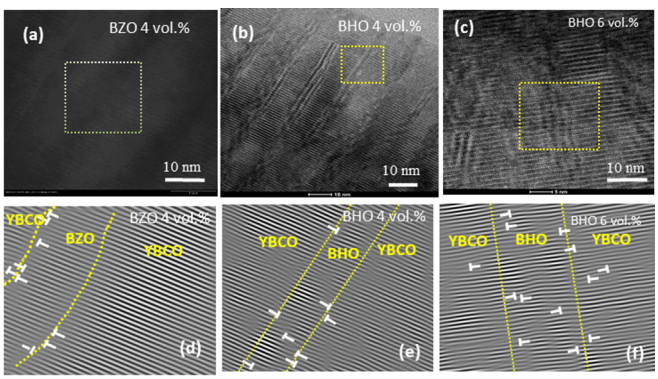

FIG. 1. Cross sectional HRTEM images of YBCO nanocomposite thin films doped with (a) 4 vol. % BZO, (b) 4 vol. % BHO, (c) 6 vol. % BHO (top row), and (d), (e), and (f) are fast Fourier filtered images of the marked area (rectangles) in (a), (b), and (c), respectively.

a similar microstructure can be observed in the 6 vol. % BHO 1D-APC/YBCO nanocomposite film in Figs. 1(c) and 1(f). This observation supports the argument of a higher elastic adaptability and smaller lattice mismatch of BHO 1D-APCs with YBCO as opposed to the BZO 1D-APC case. It would favor a more coherent 1D-APC/YBCO interface for BHO/YBCO nanocomposite films due to the compromise of the BHO and YBCO lattices. Therefore, the difference in the BZO 1D-APC/YBCO and BHO 1D-APC/YBCO interfaces has a profound effect on the strain field distribution in the nanocomposites, resulting in the different n* (and hence H^*) vs APC doping trends in these two types of 1D-APC/YBCO nanocomposites. While the microscopic mechanism underlying the difficulties in the doping higher concentration of BHO requires further investigation, Hf incorporation to the YBCO lattice, especially when YBCO is under a higher lattice strain at a higher BHO doping due to the coherent BHO/YBCO interface, may prevent formation of the BHO 1D-APCs with concentrations proportional linearly to the BHO doping levels. This argument seems consistent with the significantly reduced T_c of the 6 vol. % BHO 1D-APC/YBCO nanocomposite films as compared to their counterparts of lower BHO doping and therefore J_c measured at temperatures close to T_c.[3,15]

The difference in the interfaces of the BZO 1D-APC/YBCO and BHO 1D-APC/YBCO also impacts the pinning efficiency of these 1D-APCs. While intuitively the individual BHO and BZO 1D-APCs of comparable morphology and dimension are anticipated to have a comparable pinning efficiency, the transport $J_c(H)$ measurement confirms that this is certainly not the case. Figure 2 compares the $J_c(H)$ and $F_p(H)$ curves measured on 2, 4, and 6 vol. % BZO 1D-APC/YBCO (black) and 2 and 4 vol. % BHO 1D-APC/YBCO (red) films at $\theta = 0°$ (H//c-axis) at 77 K [Figs. 2(a) and 2(c)] and 65 K [Figs. 2(b) and 2(d)], respectively. The $J_c(H)$ curve for the undoped YBCO film (blue) is also included as a reference. A major difference in the $J_c(H)$ curves of the nanocomposite films and reference YBCO film is that the nanocomposite film

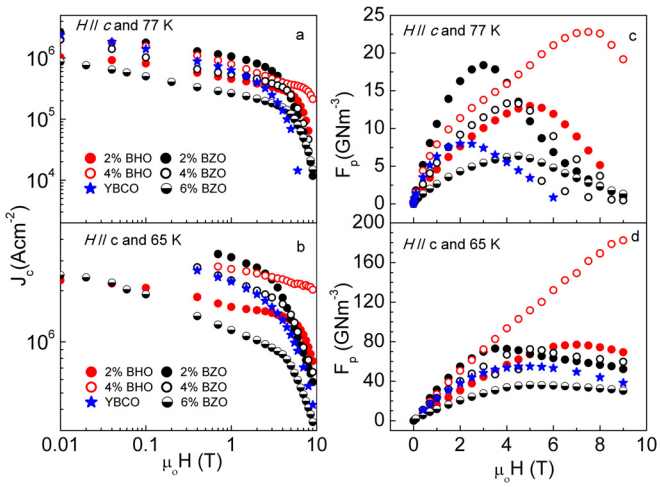

FIG. 2. J_c (H) and F_p(H) curves measured on reference YBCO (blue) and BZO 1D APC/YBCO (black) and BHO 1D-APC/YBCO (red) nanocomposite films at $\theta \sim 0°$ (H//c-axis) at 77 K (a) and (c) and (b) and (d) at 65 K, respectively. Symbols are 2% (solid), 4% (open), and 6% (half filled) in all figures.

has smaller susceptibility of $J_c(H)$ to the applied H field especially in the higher field range, which is anticipated from the improved pinning by the 1D-APCs. For quantitative comparison, the α-values were estimated from the fitting of the $J_c(H)$ curves by $J_c(H) \sim H^{-\alpha}$. At 77 K, the α-values in the range of 0.23–0.30 for almost all nanocomposite films are considerably lower than the typical value $\alpha \sim 0.5$ for the undoped YBCO reference film [Fig. 2(a)], confirming the strong correlated pinning by BZO and BHO 1D-APCs. At 65 K, significantly lower α values ∼0.10–0.11 are obtained for 2%–4% BHO 1D-APC/YBCO films as compared to α values of 0.17–21 for 2%–6% BZO 1D-APC/YBCO films and the α value of 0.25 for the reference YBCO film (Table S2). Considering that the T_c effect is negligible at 65 K, the lower α values for the BHO/YBCO nanocomposite films suggest a higher pinning efficiency of the BHO 1D-APCs than their BZO counterparts.

Moreover, opposite trends of $J_c(H)$ values are observed in the BZO/YBCO and BHO/YBCO nanocomposites with the increasing APC doping. In the former, the $J_c(H)$ curve decreases monotonically with the BZO doping in most field range, while in the latter, the $J_c(H)$ curve peaks at 4% BHO doping with lower $J_c(H)$ at the 2 vol. % and the 6 vol. % BHO doping at both 77 and 65 K [Figs. 2(a) and 2(b)]. In fact, $J_c(H)$ for the 6 vol. % BHO/YBCO film is not shown since the value is low at about 6×10^4 MA/cm^2 at 65 K and self-field, nearly two orders of magnitude lower than the other nanocomposite films in this study. In the BZO/YBCO case, a crossover between the $J_c(H)$ curves for the 2 and 4 vol. % BZO/YBCO films occurs at 4.5 T at 77 K; otherwise, an overall higher performance is observed in the lower BZO doped films. This explains the highest $F_p(H)$ curve for the 2 vol. % BZO/YBCO film at both 77 and 65 K [Figs. 2(c) and 2(d)] and a similar decreasing trend of the $F_p(H)$ curve with the increasing BZO doping, which is consistent with the previous report.[15] In comparison to the reference YBCO sample, the 2 and 4 vol. % BZO/YBCO films exhibit advantages of a significantly higher $F_p(H)$. The maximum F_p ($F_{p,max}$) in the 2 vol. % BZO/YBCO film is 18.4 and 73.1 GN/m^3 at 77 and 65 K, respectively, which is higher than $F_{p,max} \sim 8.0$ GN/m^3 and 55.0 GN/m^3 of undoped YBCO at the same temperature, while the $F_{p,max}$ for the 6 vol. % BZO/YBCO film is comparable or lower than that of the reference YBCO (Table S2). $F_{p,max}$ values of ∼13.3 GN/m^3 and 72.4 GN/m^3 for 4% BZO/YBCO are higher than those for the reference YBCO film at 77 and 65 K, respectively, and are consistent with the reported result for the comparable BZO doping.[3] In Fig. S2, a schematic of the superconducting order parameter $|\phi|$ as a function of the distance from the BZO 1D-APC is illustrated. Around a BZO 1D-APC, there are two concentric YBCO columns based on the HRTEM study.[14] The larger column of $T_{c1} < T_{c,YBCO}$ (the T_c of the original YBCO) is primarily due to the strain originated from the BZO/YBCO lattice mismatch in the c-axis. The even lower T_{c2} in the smaller column is primarily attributed to the defects/disorders especially oxygen deficiencies. This means that the pinning well height (red) and hence the pinning efficiency of the BZO 1D-APC would be much reduced. On the other hand, this inner column will not be present around the BHO 1D-APC with a coherent interface with YBCO, resulting in a higher pinning well height (black) and therefore higher pinning efficiency by BHO 1D-APCs.

In a sharp contrast, increasing $J_c(H)$ and $F_p(H)$ were observed for BHO/YBCO nanocomposite films from low to moderate BHO doping of 4 vol. %, followed by a dramatic decrease in both at 6 vol. % (Fig. 2). A similar trend of $J_c(H)$ with increasing BHO doping in the BHO/YBCO film is reportd in Refs. 3 and 16 except for 6 vol. % BHO/YBCO in which $J_c(H)$ is significantly lower in this study. It is possibly due to the severe deformation of the YBCO lattice as evidenced in the siginificant T_c decreasing to 78.5 K by maintaining the coherent BHO 1D-APC/YBCO interface to 6 vol. % BHO/YBCO or simply in 6 vol. % BHO/REBCO thin films.[17] The $F_{p,max}$ of ∼22.8 and >182 GN/m^3 (instrument limit on the maximum H field) observed at 77 and 65 K, respectively, for the 4 vol. % BHO/YBCO film is considerably higher than the best reported on BZO/YBCO nanocomposite films and the reference YBCO film as well. At 65 K, the $F_{p,max}$ of >182 GN/m^3 for the 4 vol. % BHO/YBCO film is about 2.5 times higher than the best $F_{p,max}$ of 73–74 GN/m^3 for the BZO/YBCO nanocomposte films reported in this work and by others.[15] This is the best $F_{p,max}$ reported so far at 65 K and is about 1.5 times, 1.8 times, and 1.5 times higher than the highest claimed $F_{p,max} \sim 120$ GN/m^3 for BHO/REBCO, $F_{p,max} \sim 103$ GN/m^3 for BSO/YBCO,[6,18] and $F_{p,max} \sim 122$ GN/m^3 for double perovskites (5.0 mol. % BaNbOy plus 5.0 mol. % Y_2O_3)/YBCO nanocomposite films, respectively.[19] A summary of the best reported results in the nanocomposite films with different types of 1D-APCs is given in Table S3.

In order to gain further insights into the difference in the $F_p(H)$ behviors of the two sets of the samples, H_{max} (at which the $F_{p,max}$ is observed) values are calculated and compared with the H^* estimated from the TEM in Table S2. Overall, the discrepancy is remarkable. For example, the BZO/YBCO films at 65–77 K, the H_{max} values of 3.0–3.5 T, 4.0–5.0 T, and 4.5–5.0 T at 2, 4, and 6 vol. % BZO doping are considerably lower than the H^* values of 5.0, 9.2, and 14.3 T projected from the inter 1D-APC spacing in Fig. S3. This suggests that a significant portion of the BZO 1D-APCs are not efficient pins. The trend in the BHO/YBCO case seems opposite. For the 2 vol. % BHO/YBCO film, the H_{max} value of 5.0–7.0 T at 77–65 K is more than twice of $H^* \sim 2.0$ T. At 4 vol. % BHO doping, the H_{max} value of >9.0 T (instrument limit) seems consistent to the projected H^* of 12.2 T. It should be noted that these H_{max} values are considerably higher than their BZO/YBCO counterparts. For example, at 77 K, the H_{max} value of ∼7.5 T for the 4% BHO/YBCO film is about two times higher than the H_{max} value of ∼4.0 T for the 4 vol. % BZO/YBCO film. This, together with the observed higher $F_{p,max}$, suggests higher pinning efficiency of BHO 1D-APCs than their BZO counterparts.

Figures 3(a) and 3(b) compare the H_{max}/H^* and $F_{p,max}$ values with respect to the BZO (BHO) doping concentration in BZO/YBCO (black) and BHO/YBCO (red) nanocomposite films at 77 K (solid) and 65 K (open). The numerical value of H_{max}/H^* provides the quantitative evaluation of the pinning efficiency of BZO (BHO) 1D-APCs. The H_{max}/H^* value closer to one indicates the anticipated pinning efficiency, assuming that each 1D-APC observed in the TEM

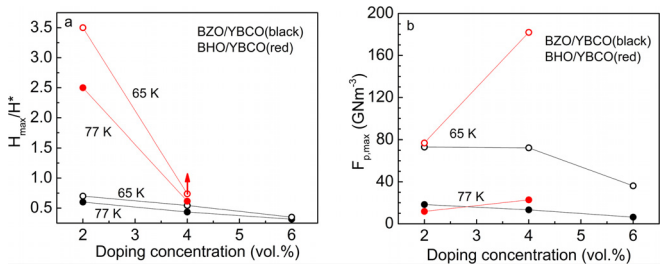

FIG. 3. APC doping concentration dependence of (a) the H_{max}/H^* ratio and (b) $F_{p,max}$ for the BZO 1D-APC/YBCO (black) and BHO 1D-APC/YBCO (red) nanocomposites at 77 K (solid) and 65 K (open), respectively, at the field orientation of the *H*//c-axis. The arrow indicates that the real value of the H_{max}/H^* ratio is expected to be higher than the data point calculated using the instrument upper limit of 9.0 T as H_{max}.

analysis can indeed pin a vortex. This value decreases with BZO (BHO) doping at both temperatures of 77 and 65 K, even though the H_{max} value increases with the doping concentration (Table S2). Specifically, the H_{max}/H^* value of BZO 1D-APCs is about 60%–70%, 43%–54%, and 31%–35% for 2, 4, and 6 vol. % BZO/YBCO films in the temperature range of 65–77 K, respectively. This means that the H_{max} value does not increase at the same rate as H^* which indicates that the proportion of effective pins reduces with increasing BZO APC doping. In contrast, the H_{max}/H^* values are significantly higher in the BHO/YBCO films. At 2 vol. % BHO, it is 250%–350%, and at 4 vol. % BHO, it reduces to 61%–>74% (partly due to the instrument limit of 9.0 T, this is inadequate to determine the H_{max} value at 65K). In contrast to BZO/YBCO, $F_{p,max}$ for BHO/YBCO increases with BHO doping to 4 vol. %. The high H_{max}/H^* value exceeding 100% suggests that a strong BHO 1D-APC could pin multiple vortices on the vortex lattice on which an elastic interaction is present between vortices.[20]

Figure 4 compares the $J_c(\theta)$ curves measured on the reference YBCO (blue), 4 vol. % BZO/YBCO (black), and 4 vol. % BHO/YBCO (red) nanocomposite films at 1.0 T [Fig. 4(a)] and 3.0 T [Fig. 4(b)] at 77 K and 5.0 T [Fig. 4(c)] and 9.0 T [Fig. 4(d)] at 65 K, respectively. In the YBCO film, the large J_c peak at 90° (*H*//ab-plane) is attributed to the intrinsic pinning. Interestingly, this J_c peak of the intrinsic pinning is nearly unaffected in the BHO/YBCO film, in

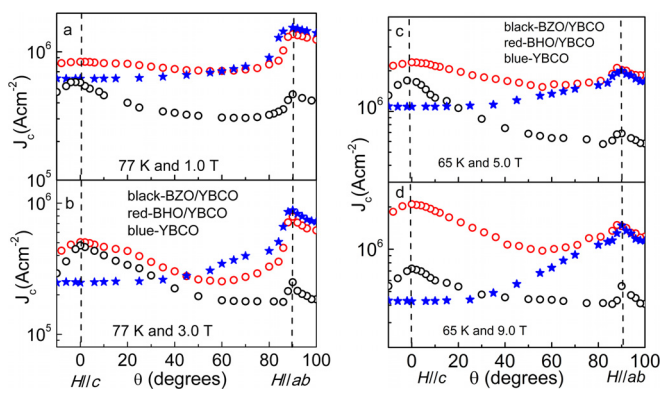

FIG. 4. Angular dependence of J_c measured on 4 vol. % BZO 1D-APC/YBCO (black) and 4% BHO 1D-APC/YBCO (red) and reference YBCO films (blue) at (a) 1.0 T, 77 K; (b) 3.0 T, 77 K, (c) 5.0 T, 65 K; and (d) 9.0 T, 65 K.

contrast to the significantly suppressed in the BZO/YBCO one. This indicates that the long-range buckling of the *ab*-planes in the BHO/YBCO nanocomposite due to the coherent BHO/YBCO interface remains effective in pin vortices as in the original YBCO. The J_c peaks at the *H*//*c*-axis for the nanocomposite films are attributed to correlated pinning by the *c*-axis aligned 1D-APCs. While these peaks are comparable at 77 K for the two films, they differ considerably at 65 K with significantly higher values observed on the BHO/YBCO film. This higher J_c-peak at the *H*//*c*-axis, in combination with the higher J_c-peak at the *H*//*ab*-plane, also leads to an overall higher $J_c(\theta)$ for the BHO/YBCO nanocomposite film as compared to the reference YBCO and BZO/YBCO nanocomposite films at 5–9 T.

In summary, this work investigates the microstructure and transport J_c in 2–6 vol. % BZO 1D-APC/YBCO and BHO 1D-APC/YBCO nanocomposite films to probe the correlation between the 1D-APC/YBCO interface and the pinning efficiency of the 1D-APCs. Several interesting insights have been obtained. First, a highly coherent BHO 1D-APC/YBCO interface can form when the BHO and YBCO lattices compronise to each other due to low rigidity of the BHO 1D-APCs and their smaller lattice mismatch with YBCO. In contrast, the less adaptive BZO 1D-APC is prone to the interface defects, resulting in a semi-coherent BZO 1D-APC/YBCO interface. Second, the 1D-APC/YBCO interface directly affects the strain field distribution around the 1D-APC in the nanocomposite films, which in turn affects the linear range of the areal concentrations of n^*_{BHO} and n^*_{BZO} (and hence the corresponding accommodation field H^*'s) vs. APC doping. The compromise of the BHO and YBCO lattices around the coherent BHO 1D-APC/YBCO interface leads to long-range *ab*-plane buckling even at 6 vol. % BHO doping, but the highly strained lattice prevents the linear increase in the BHO 1D-APC concentration with BHO doping. This is in contrast to the short-range strained lattice due to strain release via the defective semi-coherent interface around the BZO 1D-APCs, which allows n^*_{BZO} to increase linearly with the BZO doping >6 vol. %. Third, the 1D-APC/YBCO interface has a critical effect on their pinning efficiency, illustrated both in the $F_{p,max}$ value and H_{max}/H^* ratio. The BHO 1D-APCs with a coherent 1D-APC/YBCO interface have significantly higher pinning efficiency than the BZO 1D-APCs despite the two having similar 1D-APC diameters. At 65 K, for example, the former exhibits $F_{p,max}$ up to ~182 GN/m^3, which is 2.5 times of the best of 73.1 GN/m^3 by the latter. Moreover, the H_{max}/H^* ratio in the BHO 1D-APC is consistently higher than the BZO 1D-APCs. In particular, the low H_{max}/H^* ratio of <1 and the monotonic decrease in the ratio from 0.7 at 2 vol. % BZO to 0.3 at 6 vol. % BZO doping indicate that a large portion of the formed BZO 1D-APCs are inefficient in pinning. This can be explained by the significant degradation of the superconductivity in the defective BZO 1D-APC/YBCO interface column of 1–2 nm in thickness due to the severe oxygen deficiency and J_c reduction to ~60 K. This result reveals the critical importance of a high quality 1D-APC/HTS interface in achieving high pinning efficiency of the 1D-APCs.

See supplementary material for sample preparation and microstructure characterization using X-ray diffraction (XRD) and HRTEM and also three tables that summarize the details of the BZO and BHO 1D APCs and their pinning properties.

This research was supported in part by NSF contract Nos. NSF-DMR-1337737 and NSF-DMR-1508494, the AFRL Aerospace Systems Directorate, the Air Force Office of Scientific Research (AFOSR), and the U.S. National Science Foundation (DMR-1565822) for TEM characterization.

[1]C. Senatore, C. Barth, M. Bonura, M. Kulich, and G. Mondonico, Supercond. Sci. Technol. **29**(1), 014002 (2015); V. Selvamanickam, M. Heydari Gharahcheshmeh, A. Xu, E. Galstyan, L. Delgado, and C. Cantoni, Appl. Phys. Lett. **106**(3), 032601 (2015); S. Awaji, R. Ishihara, K. Watanabe, K. Shikimachi, N. Hirano, and S. Nagaya, Appl. Phys. Express **4**(1), 13101 (2011); B. Gautam, M. A. Sebastian, S. Chen, T. J Haugan, W. Zhang, J. Huang, H. Wang, and J. Z. Wu, Supercond. Sci. Technol. **31**(2), 025008 (2018); V. Chepikov, N. Mineev, P. Degtyarenko, S. Lee, V. Petrykin, A. Ovcharov, A. Vasiliev, A. Kaul, V. Amelichev, and A. Kamenev, Supercond. Sci. Technol. **30**(12), 124001 (2017).
[2]J. Wu and J. Shi, Supercond. Sci. Technol. **30**(10), 103002 (2017).
[3]T. Horide, K. Taguchi, K. Matsumoto, N. Matsukida, M. Ishimaru, P. Mele, and R. Kita, Appl. Phys. Lett. **108**(8), 082601 (2016).
[4]R. L. S. Emergo, F. J. Baca, J. Z. Wu, T. J. Haugan, and P. N. Barnes, Supercond. Sci. Technol. **23**(11), 115010 (2010); A. Llordes, A. Palau, J. Gázquez, M. Coll, R. Vlad, A. Pomar, J. Arbiol, R. Guzman, S. Ye, and V. Rouco, Nat. Mater. **11**(4), 329 (2012); V. I. Matsui, V. S. Flis, V. O. Moskaliuk, A. L. Kasatkin, N. A. Skoryk, and V. L. Svechnikov, J. Nanosci. Nanoeng. **1**(2), 38 (2015); K. Matsumoto and P. Mele, Supercond. Sci. Technol. **23**(1), 014001 (2009); S. Chen, M. Sebastian, B. Gautam, J. Wilt, T. Haugan, Z. Xing, and J. Wu, IEEE Trans. Appl. Supercond. **27**(4), 1 (2017).
[5]A. K. Jha, K. Matsumoto, T. Horide, S. Saini, P. Mele, Y. Yoshida, and S. Awaji, Supercond. Sci. Technol. **27**(2), 25009 (2014).
[6]P. Mele, K. Matsumoto, A. Ichinose, M. Mukaida, Y. Yoshida, S. Horii, and R. Kita, Physica C **469**(15), 1380 (2009).
[7]P. Pahlke, M. Lao, M. Eisterer, A. Meledin, G. Van Tendeloo, J. Hänisch, M. Sieger, A. Usoskin, J. Strömer, and B. Holzapfel, IEEE Trans. Appl. Supercond. **2**(3), 1 (2016); M. Erbe, J. Hänisch, R. Hühne, T. Freudenberg, A. Kirchner, L. Molina-Luna, C. Damm, G. Van Tendeloo, S. Kaskel, and L. Schultz, Supercond. Sci. Technol. **2**(11), 114002 (2015); H. Tobita, K. Notoh, K. Higashikawa, M. Inoue, T. Kiss, T. Kato, T. Hirayama, M. Yoshizumi, T. Izumi, and Y. Shiohara, Supercond. Sci. Technol. **25**(6), 062002 (2012).
[8]L. Opherden, M. Sieger, P. Pahlke, R. Hühne, L. Schultz, A. Meledin, G. Van Tendeloo, R. Nast, B. Holzapfel, and M. Bianchetti, Sci. Rep. **6**, 21188 (2016).
[9]B. Gautam, M. A. Sebastian, S. Chen, J. Shi, T. Haugan, Z. Xing, W. Zhang, J. Huang, H. Wang, and M. Osofsky, AIP Adv. **7**(7), 075308 (2017).
[10]J. J. Shi and J. Z. Wu, Philos. Mag. **92**(23), 2911 (2012).
[11]Y. Yoshida, S. Miura, Y. Tsuchiya, Y. Ichino, S. Awaji, K. Matsumoto, and A. Ichinose, Supercond. Sci. Technol. **30**(10), 104002 (2017).
[12]J. Z. Wu, J. J. Shi, J. F. Baca, R. Emergo, T. J. Haugan, B. Maiorov, and T. Holesinger, Supercond. Sci. Technol. **27**(4), 044010 (2014).
[13]J. Z. Wu, J. J. Shi, F. J. Baca, R. Emergo, J. Wilt, and T. J. Haugan, Supercond. Sci. Technol. **28**(12), 125009 (2015); J. Z. Wu, J. J. Shi, F. J. Baca, R. Emergo, A. Elliot, J. Wilt, M. A. Sebastian, T. Haugan, and C. V. Varanasi, IEEE Trans. Appl. Supercond. **25**, 1 (2014).
[14]C. Cantoni, Y. Gao, S. H. Wee, E. D. Specht, J. Gazquez, J. Meng, S. J. Pennycook, and A. Goyal, ACS Nano **5**(6), 4783 (2011).
[15]S. H. Wee, Y. L. Zuev, C. Cantoni, and A. Goyal, Sci. Rep. **3**, 2310 (2013).
[16]S. Miura, Y. Yoshida, Y. Ichino, K. Matsumoto, A. Ichinose, and S. Awaji, Supercond. Sci. Technol. **28**(6), 065013 (2015).
[17]K. Matsumoto, M. Nishihara, T. Kimoto, T. Horide, A. K. Jha, Y. Yoshida, S. Awaji, and A. Ichinose, Supercond. Sci. Technol. **30**(10), 104006 (2017).
[18]S. Miura, Y. Yoshida, Y. Tsuchiya, Y. Ichino, S. Awaji, A. Ichinose, K. Matsumoto, A. Ibi, T. Izumi, and M. Iwakuma, Appl. Phys. Express **10**(10), 103101 (2017).
[19]D. M. Feldmann, T. G. Holesinger, B. Maiorov, S. R. Foltyn, J. Y. Coulter, and I. Apodaca, Supercond. Sci. Technol. **23**(9), 095004 (2010).
[20]A. K. Jha, K. Matsumoto, T. Horide, S. Saini, P. Mele, A. Ichinose, Y. Yoshida, and S. Awaji, Supercond. Sci. Technol. **28**(11), 114004 (2015).